C. R. Physique 12 (2011) 4–12

Contents lists available at ScienceDirect

Comptes Rendus Physique

www.sciencedirect.com

Few body problem / Problème à petit nombre de corps

Study of Efimov physics in two nuclear-spin sublevels of ^{7}Li

Étude de l'effet d'Efimov dans deux états de spin nucléaire du ^{7}Li

Noam Gross [a], Zav Shotan [a], Olga Machtey [a], Servaas Kokkelmans [b], Lev Khaykovich [a,*]

[a] *Department of Physics, Bar-Ilan University, Ramat-Gan, 52900 Israel*
[b] *Eindhoven University of Technology, P.O. Box 513, NL-5600 MB Eindhoven, The Netherlands*

ARTICLE INFO

Article history:
Available online 6 January 2011

Keywords:
Efimov effect
Feshbach resonance
Nuclear spin

Mots-clés :
Effet d'Efimov
Résonance de Feshbach
Spin nucléaire

ABSTRACT

Efimov physics in two nuclear-spin sublevels of bosonic lithium is studied and it is shown that the positions and widths of recombination minima and Efimov resonances are identical for both states within the experimental errors, which indicate that the short-range physics is nuclear-spin independent. We also find that the Efimov features are universally related across Feshbach resonances. These results crucially depend on careful mapping between the scattering length and the applied magnetic field which we achieve by characterization of the two broad Feshbach resonances in the different states by means of rf-spectroscopy of weakly bound molecules. By fitting the binding energies numerically with a coupled channels calculation we precisely determine the absolute positions of the Feshbach resonances and the values of the singlet and triplet scattering lengths.

RÉSUMÉ

On présente une étude expérimentale de l'effet d'Efimov dans deux états de spin nucléaire du lithium bosonique, et l'on montre que les positions et les largeurs des résonances d'Efimov sur le taux de recombinaison sont les mêmes pour les deux états à l'incertitude des mesures près, ce qui indique que la physique à courte portée ne dépend pas du spin nucléaire. On trouve également que les paramètres clés de la physique d'Efimov obéissent aux relations universelles attendues sur toute la résonance de Feshbach. Ces résultats dépendent crucialement de la connnaissance de la longueur de diffusion en fonction du champ magnétique, déduite d'une caractérisation des deux résonances de Feshbach larges dans les différents états par spectroscopie radio-fréquence des états moléculaires faiblement liés. En ajustant les énergies de liaison à l'aide d'un modèle numérique à voies couplées, on détermine les positions absolues des résonances de Feshbach and les valeurs des longueurs de diffusion singulet et triplet.

1. Introduction

The recent years' remarkable progress in the study of Efimov quantum states in ultracold atoms has renewed a great deal of interest in this "old-new" quantum few-body problem. Since the first prediction made by V. Efimov in the early

* Corresponding author.
E-mail address: hykovl@mail.biu.ac.il (L. Khaykovich).

1631-0705/$ – see front matter
doi:10.1016/j.crhy.2010.10.004

1970s [1], many systems were considered for an experimental study of these quantum states; however, all of them were attempted in vain. The first experimental evidence of Efimov physics was reported in 2006 in a system of ultracold ^{133}Cs atoms [2] which was later on enhanced and verified in an additional study of the same system [3]. Since then, signatures of Efimov physics have been observed in other ultracold atomic species which turn out to be the only platform up to now suitable to study this phenomenon.

It is well known that at very low collision energies the only partial wave contributing to the scattering process is the s-wave and thus the two-body interaction is completely determined by the s-wave scattering length a. When a exceeds the characteristic two-body potential range r_0, weakly bound three-body Efimov states emerge and their number scales logarithmically with a, $N_b = (s_0/\pi)\ln(|a|/r_0)$ where $s_0 = 1.00624$ [1]. When $|a| \to \pm\infty$, the number of bound states goes to infinity and their energies are related in powers of a universal scaling factor $\exp(-2\pi/s_0) \approx 1/(22.7)^2$ [1,4]. A first indirect evidence of two consecutive Efimov states was demonstrated in ultracold ^{39}K [5] and a universal scaling across a region of $|a| \to \pm\infty$ was verified in ^{7}Li [6].

Studies of Efimov physics have been rapidly extended beyond the spin polarized bosonic samples. A notable example of a three-fermion system, all in different spin states, has been shown by a number of experimental groups [7–9] one of which developed a new and promising experimental approach to probe directly the Efimov quantum states [10]. Another example of a different system is heteronuclear universal trimers observed in Ref. [11].

Recent developments extended the universal few-body physics to the domain of four-body states which was theoretically predicted [12,13] and experimentally verified [14]. Many three- and four-body features over a large dynamical range have been demonstrated in ^{7}Li in Ref. [15]. Interestingly, the universal few-body physics can be extended to N-body clusters [16] though their experimental confirmation remains obscure.

In this work we summarize our study of Efimov physics in two different energy sublevels and across two different Feshbach resonances of the same atomic system [6,17]. As both Feshbach resonances occur at high magnetic fields where nuclear and electronic spins are decoupled, the two energy sublevels are associated with two nuclear-spin states. Our main finding is that the Efimov features are identical within the experimental errors in these two states. The absolute location and lifetime of an Efimov state is defined by the unknown short-range part of the three-body potential. Most generally, the short range potential is given in terms of two-body potential permutations of the two-body subsystems and a true three-body potential which is of importance only when three particles are very close together. It is very difficult to solve the short-range physics exactly, and therefore this region is usually treated in terms of a three-body parameter [4,18]. Thus, our results should be interpreted as a proof that the three-body parameter (and thus the short range physics) is identical for the two states. We provide new and accurate characterizations of Feshbach resonances on both states and reevaluate our previously published results in accordance with this study. Though small changes in the positions of the Efimov features can be identified, the main conclusion is not affected.

This article is organized as follows. Study of Efimov physics across two different Feshbach resonances in two nuclear-spin states is reported in Section 2. We start by comparing the relevant properties of the two energy levels and their resonances. Then, after a description of the experimental procedure we report on newly fitted positions and widths of the Efimov features based on our most recent and precise characterization of the Feshbach resonances on both nuclear-spin states. The latter is based on fitting of the binding energies of weakly bound molecular states, obtained by RF spectroscopy, to a coupled channels calculation locally for each resonance and globally for both resonances. This study is crucial for an accurate mapping of the magnetic field to the scattering length and it is considered in Section 3. Finally, Section 4 concludes the paper.

2. Efimov physics across Feshbach resonances

2.1. Comparison between two nuclear-spin states

A comprehensive discussion on the experimental characterization of Feshbach resonances will be the subject of Section 3. Here we intend to draw a general comparison between the broad resonances of the $|m_F = 1\rangle$ and the $|m_F = 0\rangle$ states of ^{7}Li in the context relevant to the study of Efimov physics. In Fig. 1(a) we show the scattering length in units of Bohr radius a_0 as a function of magnetic field in the vicinity of both Feshbach resonances with their centers aligned. It can be easily recognized that the resonances are comparable in widths while the one on the $|m_F = 0\rangle$ state is slightly wider. Although there are different hyperfine states involved, these two resonances have their origin in the same molecular bound state. Another difference is that in contrast to the $|m_F = 1\rangle$ state where only one resonance exists, on the $|m_F = 0\rangle$ state there is a second resonance overlapping with the first one. It is much narrower and is positioned by atom loss measurement at ~ 845 G [6] as shown in Fig. 1(b). We note that the measurements reported here are obtained in close vicinity to the wide resonance's position, away from the narrow one by many times its width, thus it is not expected to influence the results in the region of interest.

Signature of Efimov physics is studied here by measuring three-body recombination loss of atoms as it has been investigated in all but one recent experiments. In this respect, there is an inherent difference between the two states: in the absolute ground state, two-body relaxation mechanism is fundamentally forbidden while in the $|m_F = 0\rangle$ state it is allowed. In Fig. 2 we show the dipolar relaxation rate coefficients as a function of magnetic field which were calculated via

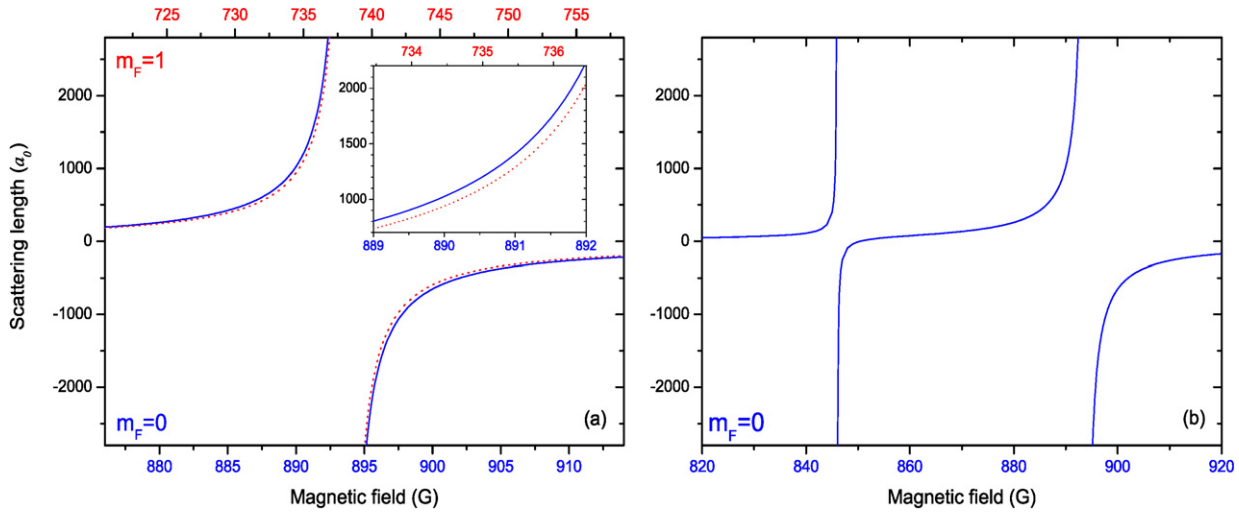

Fig. 1. (a) The broad Feshbach resonances of the $|m_F = 1\rangle$ (dashed red line) and the $|m_F = 0\rangle$ (solid blue line) states, centered at 738.2 G and 893.7 G, respectively. (b) The two Feshbach resonances of the $|m_F = 0\rangle$ state.

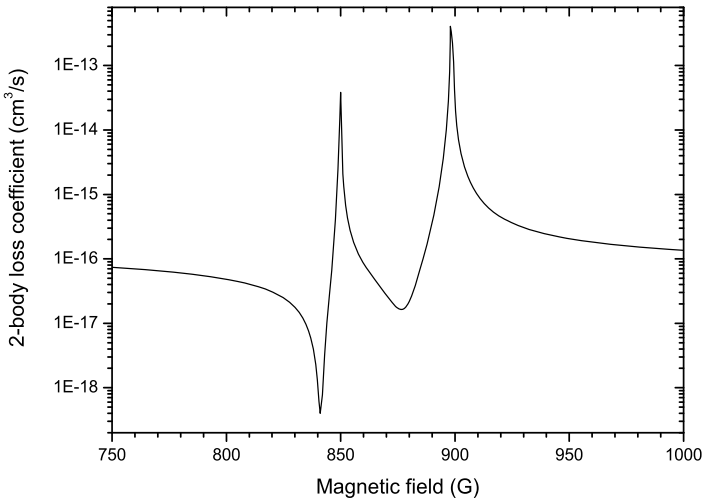

Fig. 2. A coupled-channels calculation of dipolar relaxation rate coefficients as a function of magnetic field for the $|m_F = 0\rangle$ state.

a coupled-channels calculation by using recent interaction potentials [19]. Except for two peaks which signify Feshbach resonances, the loss rate coefficients are extremely small, ~ 3 orders of magnitude smaller than the corresponding measured rate coefficients, if the experimental losses were treated as purely two-body related. For example, at 880 G the two-body loss coefficient is $\sim 5 \times 10^{-17}$ cm^3/s which yields, given that the atom density is $\sim 10^{12}$ cm^{-3}, a life time of $\sim 20\,000$ s. As a comparison, the life time in our dipole trap due to vacuum is less than 100 s. As a result, we exclude two-body losses from the analysis described below and determine that the loss processes in the region of interest are related to three-body recombination. Note that while we find this mechanism to be negligible for ^{7}Li atoms, it can be important for heavier alkali atoms. For instance, ^{133}Cs experiences large dipolar losses caused by the second-order spin–orbit interaction [20].

2.2. Experimental measurement of three-body recombination loss

According to a dimensional analysis, taking the scattering length as the only parameter describing the interaction, one finds that the three-body recombination loss rate coefficient (K_3) scales as $\hbar a^4/m$ [21]. Above this general scaling, taking into account the fact that the scattering length has to be supplemented by a three-body parameter to describe the interaction of three bosons, universal theory predicts log-periodic oscillations of K_3 due to the presence of Efimov trimer states. For positive scattering lengths the oscillations are caused by destructive interference conditions between two possible decay pathways at certain values of a [4,22]. For negative scattering lengths the loss rate coefficient exhibits a resonance enhance-

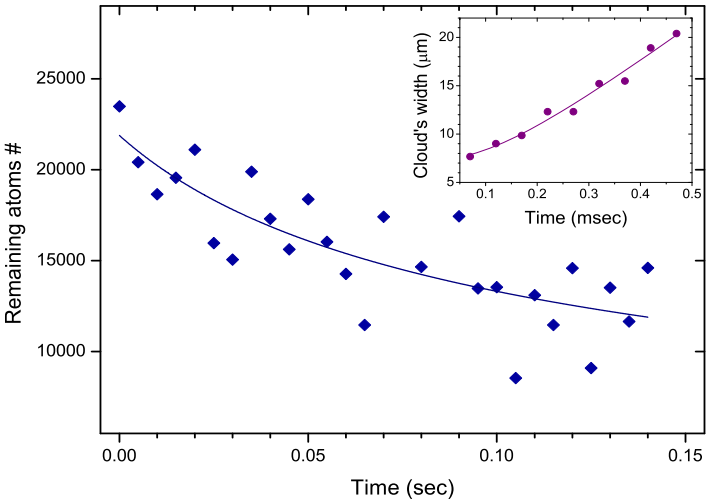

Fig. 3. A typical atom-number decay measurement on the $|m_F = 1\rangle$ state. Insert: time-of-flight measurement from which the initial temperature is deduced.

ment each time an Efimov trimer state intersects with the continuum threshold. Hence, a study of K_3 across a Feshbach resonance enables the search for an indirect evidence of Efimov trimer states.

In the experiment, we perform evaporative cooling in an optical dipole trap near a Feshbach resonance where a gas of ^{7}Li atoms is spontaneously spin purified to the $|m_F = 0\rangle$ state and is cooled down to the threshold of degeneracy [23]. For measurements in the absolute ground state ($|m_F = 1\rangle$), a rapid adiabatic passage by means of a radio-frequency (rf) sweep at a low magnetic field is used to transfer the atoms from the $|m_F = 0\rangle$ state [17]. We conduct measurements of atom-number decay and initial temperature as a function of magnetic field in the vicinity of wide Feshbach resonances on both states. An example of such set of measurements is shown in Fig. 3. We use the temperature measurement, together with a precise characterization of the trap frequencies, to estimate the initial atom density. Then, the K_3 value is extracted by fitting the atom-number decay measurement with the atom-loss rate equation solution:

$$\dot{N} = -K_3\langle n^2\rangle N - \Gamma N, \tag{1}$$

where K_3 and Γ are the three- and single-body loss rate coefficients, respectively. Γ is determined independently by measuring a very long decay tail of a low density sample. Note that this simplified model does not include several important effects, one of which is the saturation of K_3 to a maximal value K_{max} due to finite temperature (unitarity limit) and it can be represented as [24]:

$$K_{max} = c\frac{125\pi^2\hbar^5}{m^3k_B^2T^2}, \tag{2}$$

where m is the atomic mass, k_B is the Boltzmann's constant and c is a numerical constant distinguishing between the two threshold regimes of the collision energies, $c = 1$ for $a > 0$ and $c \approx 0.1$ for $a < 0$. To address this limitation, measurements for which $K_3 \gtrsim 0.1K_{max}$ are omitted from the analysis of Efimov features (see Section 2.3).

Other effects which are not included in the model are 'anti-evaporation' and recombination heating [25]. The first is an effective heating caused by a preferential loss of atoms from the densest (and thus coldest) part of the cloud. We treat the evolution of our data to no more than $\sim 30\%$ decrease in atom number, as can be seen in Fig. 3, for which 'anti-evaporation' is estimated to induce a systematic error of $\sim 23\%$ towards higher values of K_3. The error is evaluated based on an analytical solution to coupled atom-loss rate and temperature evolution equations [25,5] and it is estimated not to limit the accuracy of the reported results. Recombination heating can be neglected for $K_3 \ll K_{max}$ because in this case the trap depth (which scales with temperature) is smaller than the energy released in the recombination process leading to an immediate loss of the colliding partners. Moreover, this approach, together with the small decrease in atom number, allows time evolution of the unitarity limit ($K_{max}(t)$) to be neglected within a single atom-number decay measurement. Note, that 'anti-evaporation' and recombination heating pose strong limitations on the measurement's dynamical range in the large scattering lengths limit where more careful model than Eq. (1) has to be considered. This is demonstrated for $|m_F = 1\rangle$ state in Fig. 4 where a dramatic increase in the initial temperature of the atom-number decay measurement near the resonance corresponds to a reduction in the value of K_{max} according to Eq. (2).

2.3. Efimov features and universality

Experimental results of the three-body loss measurements are summarized in Fig. 5 where K_3 is plotted as a function of the scattering length a for the $|m_F = 1\rangle$ state (red solid circles) and the $|m_F = 0\rangle$ state (blue open diamonds). Magnetic

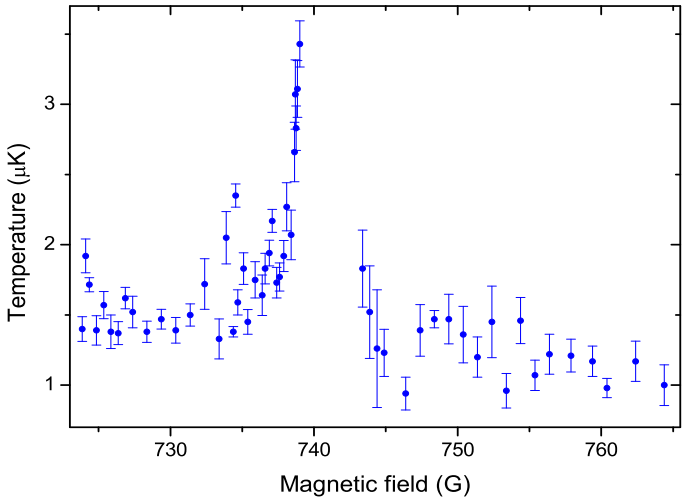

Fig. 4. Initial temperature of the atom-number decay measurement around the Feshbach resonance on the $|m_F = 1\rangle$ state from which the atom density is extracted for the calculation of K_3. Each point is deduced from a time-of-flight measurement (see insert in Fig. 3). The error bars represent the fitting errors.

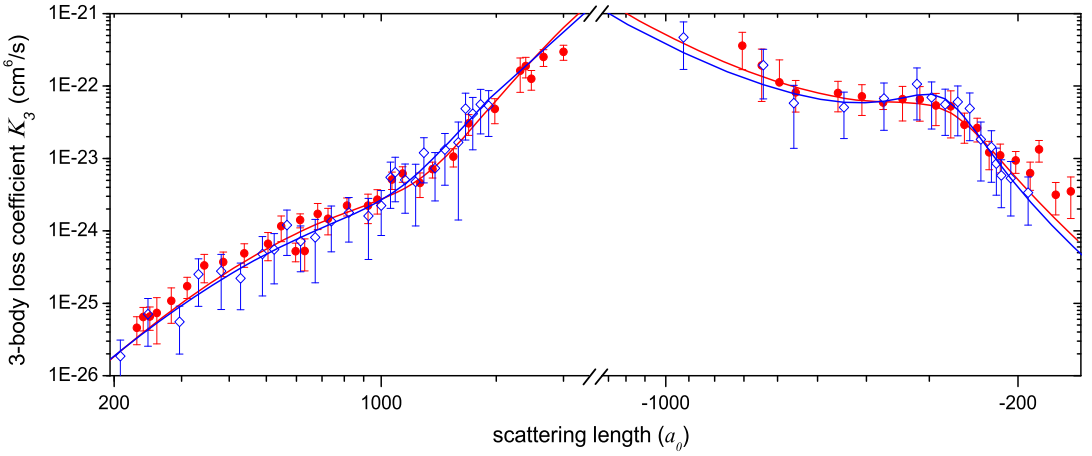

Fig. 5. Experimentally measured three-body loss coefficient K_3 as a function of scattering length (in units of Bohr radius a_0) for the $|m_F = 1\rangle$ state (red solid circles) and the $|m_F = 0\rangle$ state (blue open diamonds). The solid lines (red and blue, respectively) represent fits to the analytical expressions of universal theory.[2] The error bars consist of two contributions: the uncertainty in temperature measurement which affects the estimated atom density and the fitting error of the atom-number decay measurement.

field values are converted to scattering lengths via a careful analysis of the Feshbach resonances, that will be discussed in Section 3. A qualitative analysis indicates a striking similarity between the two sets of measurements for both positive and negative scattering lengths. We can further verify this similarity quantitatively by fitting the measured K_3 data to a prediction of universal theory. For that purpose we represent the loss rate coefficient in a convenient form [4]:

$$K_3 = 3C_{\pm}(a)\hbar a^4/m \tag{3}$$

where $\pm$ hints at the positive $(+)$ or negative $(-)$ region of the scattering length. An effective field theory provides analytic expressions for $C_{\pm}(a)$ that we use in the form represented in [2,3]:

$$C_+(a) = 67.1e^{-2\eta_+}\left(\cos^2\left[s_0\ln(a/a_+)\right] + \sinh^2\eta_+\right) + 16.8\left(1 - e^{-4\eta_+}\right) \tag{4}$$

and

$$C_-(a) = 4590\sinh(2\eta_-)/\left(\sin^2\left[s_0\ln(|a|/a_-)\right] + \sinh^2\eta_-\right), \tag{5}$$

[2] We note that the four points with the highest values of K_3 on $|m_F = 1\rangle$ $a > 0$ were omitted from the fitting procedure on the grounds of approaching the finite temperature saturation value K_{max} (unitarity limit) [24] which is $\sim 4.5 \times 10^{-21}$ cm^6/s for a temperature of 3.5 μK.

Table 1
Fitting parameters to universal theory obtained from the measured K_3 values of the $|m_F = 1\rangle$ and the $|m_F = 0\rangle$ states.

State	η_+	η_-	a_+/a_0	a_-/a_0	$a_+/\lvert a_-\rvert$
$\lvert m_F = 0\rangle$	0.213(79)	0.180(48)	238(25)	−280(12)	0.85(11)
$\lvert m_F = 1\rangle$	0.170(41)	0.253(62)	265(16)	−274(12)	0.97(8)

where the free parameters of the fits are $a_\pm$ and $\eta_\pm$ which are connected to the real and the imaginary parts of the three-body parameter, respectively [4,26]. The fitting results are represented by solid lines in corresponding colors in Fig. 5 (see footnote 2) and the fitting parameters are summarized in Table 1. Comparing corresponding parameters in different states acknowledges the notion that the Efimov features are identical within the experimental errors which signifies that the short-range physics is nuclear-spin independent. An interesting conclusion can be drawn from this observation. Recall that the short range potential is given in terms of two-body potential permutations of the two-body subsystems and a true three-body potential. As the two Feshbach resonances occur at high magnetic fields where the nuclear and electron spins are effectively decoupled, the two-body potentials are similar for both states. Therefore, if the short-range physics is spin-independent, the true three-body forces are either also nuclear-spin independent or play a relatively minor role.

Moreover, two predictions of universal theory are also verified here: first, the decay parameters η_+ and η_-, which describe the lifetime of the Efimov state, are assumed to be equal and indeed they are (within the experimental errors). This suggests that the imaginary part of the three-body parameter is identical. Second, the theoretical assumption that the real part of the three-body parameter across a Feshbach resonance is the same for negative and positive scattering length regions requires a_+ and a_- to obey a universal ratio $a_+/|a_-| = 0.96(3)$ [4]. The fits yield values of 0.85(11) and 0.97(8) for $|m_F = 0\rangle$ and $|m_F = 1\rangle$, respectively, which overlap with each other and with the predicted value within the experimental and theoretical error bars. We thus confirm that the three-body parameter is preserved across two different Feshbach resonances and between two different nuclear-spin states. Note that slight deviations of our measurements from the universally predicted values can be explained by finite effective range corrections which were recently evaluated by means of an effective field theory [27].

For positive scattering lengths, the Efimov trimer is expected to intersect with the atom-dimer threshold at $a_* \approx 1.1a_+$ [4]. Theory predicts that a_* and a_- of the same trimer state are related as $a_- \approx -22a_*$ [4]. Therefore, if the observed Efimov resonance at a_- indicates the lowest state, the one expected at a_* indicates the first excited state as the lowest one becomes nonuniversal.

3. Characterization of Feshbach resonances

3.1. Experimental measurements of binding energy of Feshbach molecules

For a correct investigation of the K_3 coefficients dependence on the two-body scattering length, it is crucial to have an accurate mapping between the scattering length and the applied magnetic field. For this purpose, the binding energies of the underlying bound states which give rise to the two broad Feshbach resonances are carefully measured using rf molecule association. This method uses a weak rf field to resonantly associate weakly bound Feshbach dimers which are then rapidly lost through collisional relaxation into deeply bound states [28]. In the experiment the rf modulation time is varied between 0.5 and 3 sec and the modulation amplitude ranges from 150 to 750 mG. The remaining atom number is measured by absorption imaging as a function of rf frequency at a given magnetic field and the rf-induced losses are then numerically fitted to a convolution of a Maxwell–Boltzmann and a Gaussian distributions. The former accounts for broadening of the spectroscopic feature due to finite kinetic energy of atoms at a typical temperature of ~ 1.5 μK [29]. The latter reflects broadening due to magnetic field instability and shot-to-shot atom number fluctuations. From the fit we extract the molecular binding energy (E_b) corresponding to zero temperature. An example of a molecule association induced loss feature is depicted in Fig. 6 where the characteristic asymmetry of the obtained profile is clearly seen [29]. Results of the binding energy rf spectroscopy for both states are shown in Fig. 7. We analyze these results by fitting them with a coupled-channels calculation which is discussed in the next section.

3.2. Analysis of two-body interactions

Very close to resonance, the binding energy is related to the scattering length as

$$E_b(a) = -\frac{\hbar^2}{ma^2}. \tag{6}$$

This expression shows that ultracold scattering physics is closely related to bound state physics just below the dissociation threshold. However, this simple relationship rapidly breaks down when going further away from resonance, and is therefore not sufficient to interpret three-body recombination in terms of the scattering length.

In order to make a correct mapping between binding energy and scattering length, we make use of a coupled-channels two-body interaction model for lithium, which has been discussed earlier [19], and we use the interaction potentials dis-

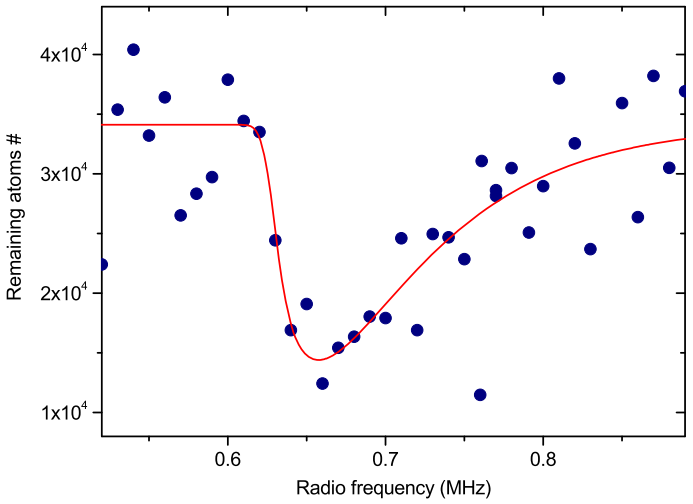

Fig. 6. rf association of molecules at $B = 734.4$ G on the $|m_F = 1\rangle$ state. The loss resonance is fitted numerically to a convolution of Maxwell–Boltzmann and a Gaussian distributions (solid line).

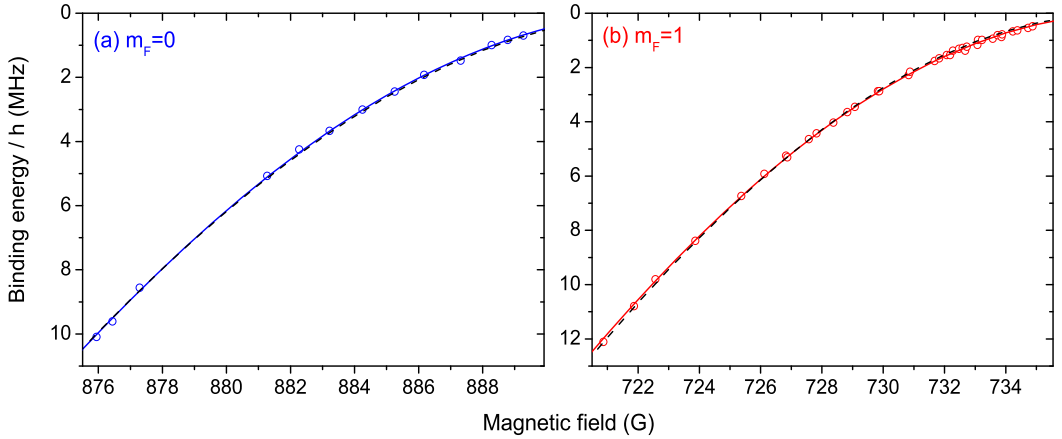

Fig. 7. rf spectroscopy of the molecular binding energy near the Feshbach resonance in the $|m_F = 0\rangle$ (a) and the $|m_F = 1\rangle$ (b) states. The solid line represents an independent fit to CC calculation while the dark dashed line is the combined fit for both states simultaneously.

cussed there as a starting point for our analysis. For large interatomic separations r the singlet ($S = 0$) and a triplet ($S = 1$) potentials are given by

$$V_S(r) = -\frac{C_6}{r^6} - \frac{C_8}{r^8} - \frac{C_{10}}{r^{10}} - (-1)^S C^{ex} r^{7/2\alpha - 1} e^{-2\alpha r}, \tag{7}$$

with van der Waals coefficients C_6, C_8, C_{10} [32], exchange parameter C^{ex} [33,34], and the ionization energy $\alpha^2/2$ [35]. For the short radial range r we use model singlet and triplet potentials which have also been used in Refs. [36,37].

The short-range and long-range potentials are smoothly connected at $r = 18a_0$. We improve the accuracies of the short range potentials considerably, by making use of the accumulated phase method [36]. Therefore a boundary condition is applied on the partial-wave radial wave functions at $r = 7a_0$ in the form of a WKB phase

$$\phi_{S,T}(E, \ell) = \phi^0_{S,T}(E, \ell) + \Delta\phi_{S,T}. \tag{8}$$

The first term on the right is calculated by radial integration of the model potential up to $7a_0$ and is sufficiently accurate to account for the energy and angular momentum dependence of the accumulated phase. The corrections $\Delta\phi_{S,T}$ to the accumulated singlet and triplet phases are independent of energy and angular momentum.

The most crucial parameters in the coupled channels model are $\Delta\phi_S$, $\Delta\phi_T$ and C_6, which we take as free parameters that we determine from our experimental binding energies. We perform a χ^2 minimization with respect to the free parameters, and this allows us to determine the positions of both Feshbach resonances, and the direct mapping of the scattering length on the magnetic field $a(B)$. In order to extract the resonance's parameters we fit $a(B)$ with a factorized expression [38]:

Table 2
Feshbach resonance parameters for both states as obtained from independent fits of the CC calculation to the molecular binding energies (solid lines in Fig. 7).

State	Type	a_{bg}/a_0	Δ (G)	B_0 (G)
$\|m_F = 0\rangle$	narrow	−18.24	+4.518	846.0
$\|m_F = 0\rangle$	wide	−18.24	−237.8	893.7(3)
$\|m_F = 1\rangle$	wide	−20.98	−171.0	738.2(2)

Table 3
Feshbach resonances' positions (B_0) as obtained from a combined fitting of the molecular binding energy measurements in both states simultaneously to the CC calculation. The experimentally determined positions are presented in the last column where the narrow resonance was determined by atom loss measurement [6] and the two wide ones where determined by independent fits of the molecular binding energies (see Table 2). The field calibration uncertainty is included in the experimental errors.

State	Type	B_0 (G)	
		Combined fit	Experimental
$\|m_F = 0\rangle$	narrow	845.54	844.9(8)
$\|m_F = 0\rangle$	wide	893.95(5)	893.7(4)
$\|m_F = 1\rangle$	wide	737.88(2)	738.2(4)

$$\frac{a}{a_{bg}} = \prod_{i=1}^{N}\left(1 - \frac{\Delta_i}{(B - B_{0,i})}\right), \tag{9}$$

where a_{bg} is the background scattering length, Δ_i is the i's resonance width and $B_{0,i}$ is the i's resonance position.

We analyze the data in two different ways. First we perform an independent fit of the model to the $|m_F = 0\rangle$ and the $|m_F = 1\rangle$ binding energies, represented by solid blue and red lines in Fig. 7(a) and (b), respectively. Then, a combined fit for both m_F states is performed (dashed black line in Fig. 7(a,b)), which allows us to check the consistency between the two different experiments, within the same interaction model. Deviations of the second case from the first one are a hint for possible different systematic shifts in magnetic field calibration for both states. This can be explained by the fact that a precise calibration of the magnetic field is performed locally by microwave transitions in the vicinity of each of the wide resonances. Note that each set of measurements is limited to a range of ± 20 G around the resonances while the distance between them is ~ 150 G. We therefore use the results of the independent fits for the K_3 analysis which was discussed previously in this paper. The resonances' parameters as obtained from the independent fits are summarized in Table 2.

Table 3 represents the resonances' positions obtained from the combined fit and compares them with our most precise to-date experimental values, i.e. an atom loss measurement for the narrow resonance of $|m_F = 0\rangle$ [6] and the two independent fits of the wide resonances (Table 2). A field calibration uncertainty of 0.3 G is added to the fitting errors of the experimental values.

We find the results in Table 3 mutually consistent. Moreover, the determined values for ϕ_S, $\Delta\phi_T$ and C_6 are all consistent with the bound of earlier performed analysis [36,30,37,19]. Since our combined analysis only weakly depends on the value of the C_6 coefficient, we present our results with a fixed value of C_6 which was found in the *ab initio* calculations [32, 31]. The determined parameters ϕ_S and $\Delta\phi_T$ correspond to the singlet and triplet scattering lengths $a_S = 34.33(2)\ a_0$ and $a_T = -26.87(8)\ a_0$.

4. Conclusions

In this work we study experimentally Efimov physics in two nuclear-spin sublevels of bosonic lithium and show that the positions and widths of recombination minima and Efimov resonances are identical for both states within the experimental errors. As the properties of Efimov features are governed by the three-body parameter, our study indicates that the short-range physics is nuclear-spin independent. We also find that the Efimov features are universally related across the Feshbach resonances. Let us note that the observed position of the Efimov resonance reveals the same numerical factor $|a_-|/r_0 \approx 8.5$ as in the experiments on ^{133}Cs [2] which may or may not be an accidental coincidence.

The reported results crucially depend on a careful mapping between the scattering length and the magnetic field. We characterize two wide Feshbach resonances in different states by fitting the binding energies of weakly bound molecules, created by rf-association, with a coupled channels analysis. This gives rise to a very precise determination of the absolute positions of the Feshbach resonances and the values of the singlet and triplet scattering length that characterize the molecular potentials of lithium.

Acknowledgements

This work was supported, in part, by the Israel Science Foundation and by the Netherlands Organization for Scientific Research (NWO). N.G. is supported by the Adams Fellowship Program of the Israel Academy of Sciences and Humanities.

References

[1] V. Efimov, Phys. Lett. B 33 (1970) 563; Sov. J. Nucl. Phys. 12 (1971) 589; Sov. J. Nucl. Phys. 29 (1979) 546.
[2] T. Kraemer, M. Mark, P. Waldburger, J.G. Danzl, C. Chin, B. Engeser, A.D. Lange, K. Pilch, A. Jaakkola, H.-C. Nägerl, R. Grimm, Nature 440 (2006) 315.
[3] S. Knoop, F. Ferlaino, M. Berninger, M. Mark, H.-C. Nägerl, R. Grimm, Nature Phys. 5 (2009) 227.
[4] E. Braaten, H.-W. Hammer, Phys. Rep. 428 (2006) 259.
[5] M. Zaccanti, B. Deissler, C. D'Errico, M. Fattori, M. Jona-Lasinio, S. Müller, G. Roati, M. Inguscio, G. Modugno, Nature Phys. 5 (2009) 586.
[6] N. Gross, Z. Shotan, S.J.J.M.F. Kokkelmans, L. Khaykovich, Phys. Rev. Lett. 103 (2009) 163202.
[7] T.B. Ottenstein, T. Lompe, M. Kohnen, A.N. Wenz, S. Jochim, Phys. Rev. Lett. 101 (2008) 203202;
A.N. Wenz, T. Lompe, T.B. Ottenstein, F. Serwane, G. Zürn, S. Jochim, Phys. Rev. A 80 (2009) 040702(R);
T. Lompe, T.B. Ottenstein, F. Serwane, K. Viering, A.N. Wenz, G. Zürn, S. Jochim, Phys. Rev. Lett. 105 (2010) 103201.
[8] J.H. Huckans, J.R. Williams, E.L. Hazlett, R.W. Stites, K.M. O'Hara, Phys. Rev. Lett. 102 (2009) 165302;
J.R. Williams, E.L. Hazlett, J.H. Huckans, R.W. Stites, Y. Zhang, K.M. O'Hara, Phys. Rev. Lett. 103 (2009) 130404.
[9] S. Nakajima, M. Horikoshi, T. Mukaiyama, P. Naidon, M. Ueda, Phys. Rev. Lett. 105 (2010) 023201.
[10] T. Lompe, T.B. Ottenstein, F. Serwane, A.N. Wenz, G. Zürn, S. Jochim, arXiv:1006.2241.
[11] G. Barontini, C. Weber, F. Rabatti, J. Catani, G. Thalhammer, M. Inguscio, F. Minardi, Phys. Rev. Lett. 103 (2009) 043201.
[12] L. Platter, H.-W. Hammer, Ulf-G. Meißner, Phys. Rev. A 70 (2004) 052101.
[13] J. von Stecher, J.P. D'Incao, C.H. Greene, Nature Phys. 5 (2009) 417.
[14] F. Ferlaino, S. Knoop, M. Berninger, W. Harm, J.P. D'Incao, H.-C. Nägerl, R. Grimm, Phys. Rev. Lett. 102 (2009) 140401.
[15] S.E. Pollack, D. Dries, R.G. Hulet, Science 326 (2009) 1683.
[16] J. von Stecher, J. Phys. B 43 (2010) 101002;
G.J. Hanna, D. Blume, Phys. Rev. A 74 (2006) 063604.
[17] N. Gross, Z. Shotan, S.J.J.M.F. Kokkelmans, L. Khaykovich, Phys. Rev. Lett. 105 (2010) 103203.
[18] J.P. D'Incao, C.H. Greene, B.D. Esry, J. Phys. B 42 (2009) 044016.
[19] E.G.M.v. Kempen, B. Marcelis, S.J.J.M.F. Kokkelmans, Phys. Rev. A 70 (2004) 050701(R).
[20] S.J.J.M.F. Kokkelmans, B.J. Verhaar, K. Gibble, Phys. Rev. Lett. 81 (1998) 951;
F.H. Mies, C.J. Williams, P.S. Julienne, M. Krauss, J. Res. Natl. Inst. Stand. Technol. 101 (1996) 521.
[21] P.O. Fedichev, M.W. Reynolds, G.V. Shlyapnikov, Phys. Rev. Lett. 77 (1996) 2921.
[22] B.D. Esry, C.H. Greene, J.P. Burke, Phys. Rev. Lett. 83 (1999) 1751;
E. Nielsen, J.H. Macek, Phys. Rev. Lett. 83 (1999) 1566.
[23] N. Gross, L. Khaykovich, Phys. Rev. A 77 (2008) 023604.
[24] J.P. D'Incao, H. Suno, B.D. Esry, Phys. Rev. Lett. 93 (2004) 123201.
[25] T. Weber, J. Herbig, M. Mark, H.-C. Nägerl, R. Grimm, Phys. Rev. Lett. 91 (2003) 123201.
[26] B. Marcelis, S.J.J.M.F. Kokkelmans, G.V. Shlyapnikov, D.S. Petrov, Phys. Rev. A 77 (2008) 032707.
[27] C. Ji, D. Phillips, L. Platter, Europhys. Lett. 92 (2010) 13003.
[28] S.T. Thompson, E. Hodby, C.E. Wieman, Phys. Rev. Lett. 95 (2005) 190404.
[29] T.M. Hanna, T. Köler, K. Burnett, Phys. Rev. A 75 (2007) 013606.
[30] E.R.I. Abraham, W.I. McAlexander, J.M. Gerton, R.G. Hulet, R. Côté, A. Dalgarno, Phys. Rev. A 55 (1997) R3299.
[31] A. Derevianko, J.F. Babb, A. Dalgarno, Phys. Rev. A 63 (2001) 052704.
[32] Z.-C. Yan, J.F. Babb, A. Dalgarno, G.W.F. Drake, Phys. Rev. A 54 (1996) 2824.
[33] W.T. Zemke, W.C. Stwalley, J. Chem. Phys. 111 (1999) 4962.
[34] M. Marinescu, A. Dalgarno, Z. Phys. D 36 (1996) 239.
[35] C.J. Lorenzen, K. Niemax, J. Phys. B 15 (1982) L139–L145.
[36] A.J. Moerdijk, B.J. Verhaar, Phys. Rev. Lett. 73 (1994) 518.
[37] F.A. van Abeelen, B.J. Verhaar, A.J. Moerdijk, Phys. Rev. A 55 (1997) 4377.
[38] A.D. Lange, K. Pilch, A. Prantner, F. Ferlaino, B. Engeser, H.-C. Nägerl, R. Grimm, C. Chin, Phys. Rev. A 79 (2009) 013622.